PROCEEDINGS OF SCIENCE

Multi-band Variability Analysis of the Blazar OJ 014

Min Jin,[a,*] **Feng-rong Zhu**[a,b] **and Bing-kai Zhang**[c,d]

[a] *School of Physical Science and Technology, Southwest Jiaotong University, Chengdu, Sichuan Province, 611756, China.*

[b] *Science School, Tibet University, Lhasa, Tibet, 850000, China.*

[c] *Department of Physics, Fuyang Normal University, Fuyang, Anhui Province, 236037, China.*

[d] *Key Laboratory of Functional Materials and Devices for Informatics Anhui Higher Education Institutes, Fuyang, Anhui Province, 236037, China.*

E-mail: jinmin@my.swjtu.edu.cn, zhufr@swjtu.edu.cn

Blazars are a subclass of active galactic nuclei (AGN) characterized by relativistic jets oriented close to our line of sight, exhibiting extreme variability across multi-band observations. This study performed variability analysis of multi-band light curves for the blazar OJ 014 (J0811.4+0146) using data from Fermi-LAT, Swift-XRT/UVOT, and RATAN observations spanning from August 2008 to November 2024. Time series analysis reveals a significant quasi-periodic oscillation (QPO) with a period of 4.35 ± 0.34 years in the γ-ray emission, detected at a significance level of $4.5\,\sigma$. Cross-correlation analysis between different energy bands was performed to investigate the relationships between multiband light variations. The spectral energy distribution across all observed frequencies exhibits the characteristic double-humped structure typical of blazars, well-described by a leptonic model dominated by synchrotron radiation and inverse Compton scattering. The detected QPO behavior can be attributed to Newtonian-driven jet precession in a Supermassive Black Hole Binary system, with estimated masses of $7.33 \times 10^9\,M_\odot$ and $2.13 \times 10^9\,M_\odot$ for the primary and secondary black holes respectively. This configuration yields a secondary black hole orbital period of 1.15 years and a jet precession period of approximately 42.49 years.

39th International Cosmic Ray Conference (ICRC2025)
15–24 July 2025
Geneva, Switzerland

ICRC 2025
The Astroparticle Physics Conference
Geneva July 15-24, 2025

*Speaker

PoS(ICRC2025)699

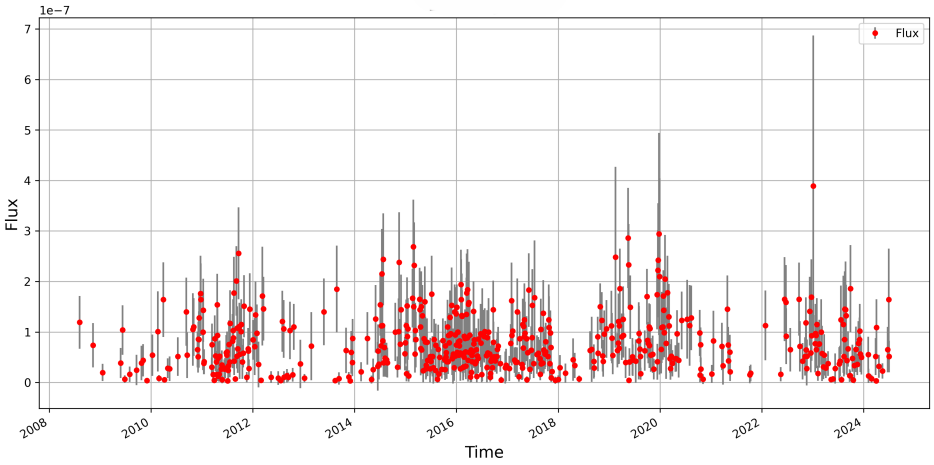

Figure 1: Light curve of J0811.4+0146. The data points are from Fermi-LAT, and the ordinate represents the photon flux measured in units of photons cm^{-2} s^{-1} in the energy range of 0.1-100 GeV. The abscissa represents the observation time.

1. Introduction

Active Galactic Nuclei (AGN) are powered by accretion onto super-massive black holes. When the relativistic jet points almost directly at Earth (within an angle $\lesssim 1/\Gamma$), the object is observed as a blazar [1, 3].

Rapid, large-amplitude variability is a defining trait, detectable from radio to γ-ray energies on timescales of minutes to years [12]. Systematic searches have uncovered quasi-periodic oscillations (QPOs) in a growing sample: PG 1553+113 exhibits a ∼2.2 yr γ-ray cycle [**?**], PKS 0537-441 shows a transient 55 d modulation [**?**], and OJ 287 maintains a long-standing ∼12 yr optical period [**?**]. A recent census reports > 11 blazars with convincing QPO signatures [**?**], highlighting the need to clarify the underlying mechanisms.

J0811.4+0146 (OJ 014). — This BL Lac object (z = 1.15) was catalogued in CRATES and later confirmed as a γ-ray blazar by *Fermi*-LAT. Its optical–radio variability has been known since the 1970s. VLBI images reveal a compact, super-luminal jet, and X-ray observations show the hard spectrum expected from a high-synchrotron-peaked source. The broadband SED exhibits the canonical double-humped structure, well explained by synchrotron and inverse-Compton processes.

Early *Fermi* data hinted at a ∼4.3 yr QPO in J0811.4+0146. With an expanded dataset (2008 – 2024), differences in reported periods and significances motivate a re-examination.

This work analyses the weekly *Fermi*-LAT light curve of J0811.4+0146 over 16 yr, applying multiple time-series techniques to test for persistent or transient periodicity. Section 2 describes data selection, Section 3 outlines the methods, Section 4 discusses the results in the context of jet dynamics and binary black-hole scenarios, and Section 5 states the conclusions.

2. Data Acquisition and Selection

This study uses Fermi-LAT 4FGL catalog data with the `gll_iem_v07.fits` interstellar emission model. Observations within a 1-degree aperture cover the 100 MeV to 100 GeV energy range.

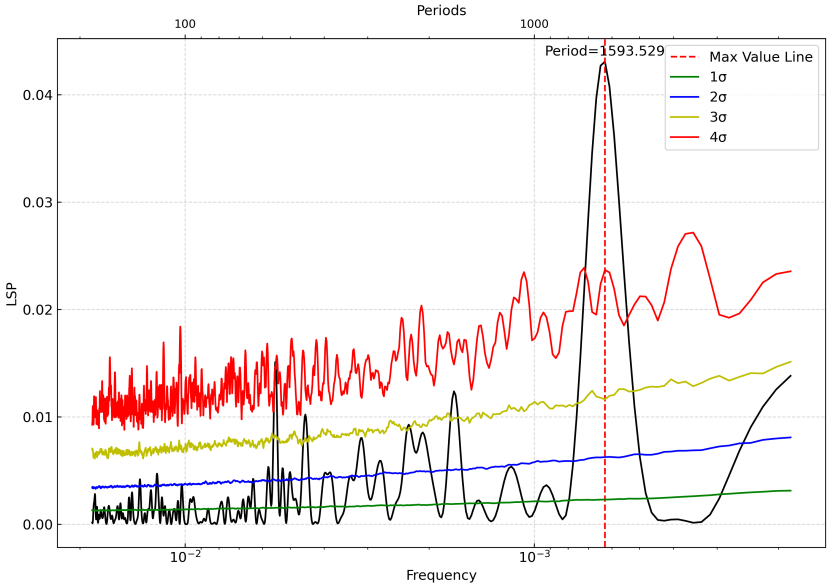

Figure 2: Lomb-Scargle Periodogram of J0811.4+0146 showing significant periodicity (1–4σ confidence curves shown).

Data filtering adheres to P8 Source class criteria (`evclass=128`, `evtype=3`) with a zenith angle limit of 90°. Periods where any source was within 5° of the Sun were excluded. Analyses primarily use the 3-day binned light curve from Fermi-tools for precision, supplemented by weekly and monthly bins.

3. Periodicity Search

Four methods are employed: Lomb-Scargle Periodogram (LSP), Weighted Wavelet Z-transform (WWZ), Discrete Correlation Function (DCF), and Jurkevich (JV).

3.1 Lomb-Scargle Periodogram (LSP)

The LSP method excels at detecting periodicities in unevenly sampled astrophysical data while providing significance estimates, though it can be sensitive to noise and aliasing. For time series data $\{t_i, y_i\}$, the power spectrum $P(\omega)$ is:

$$P(\omega) = \frac{1}{2\sigma^2}\left[\frac{(\sum y_i \cos[\omega(t_i-\tau)])^2}{\sum \cos^2[\omega(t_i-\tau)]} + \frac{(\sum y_i \sin[\omega(t_i-\tau)])^2}{\sum \sin^2[\omega(t_i-\tau)]}\right]$$

where τ satisfies $\tan(2\omega\tau) = \frac{\sum \sin(2\omega t_i)}{\sum \cos(2\omega t_i)}$.

Applied to J0811.4+0146 (Fig. 2), the LSP reveals a significant peak ($> 4.5\sigma$) at frequency 0.0006275 day^{-1}, corresponding to a period of ~1594 days.

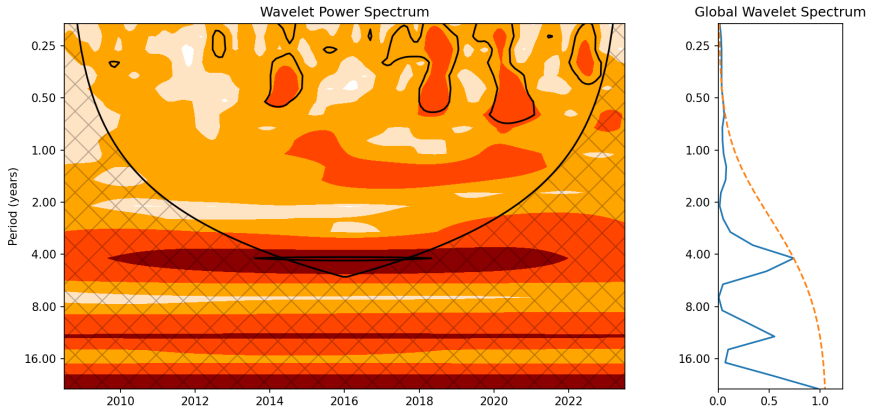

Figure 3: Weighted wavelet Z-transform (WWZ) analysis of J0811.4+0146. Left panel: Wavelet power spectrum, where the x-axis denotes time, the y-axis represents period, and color indicates normalized wavelet power spectral density. The color scale ranges from white to deep red, with increasing power as the color transitions towards deep red. The thick black contour delineates regions of > 95% confidence. Right panel: Global wavelet spectrum derived from the WWZ.

3.2 Weighted Wavelet Z-Transform (WWZ)

The WWZ analyzes non-stationary time series through localized time-frequency decomposition, identifying evolving periodic components [9]. The core transform is defined as:

$$W_n(s) = \sum_{n'=0}^{N-1} Y_{n'} \psi^* \left[\frac{(n'-n)\Delta t}{s} \right], \tag{1}$$

where $W_n(s)$ is the wavelet coefficient at time index n and scale s, $Y_{n'}$ is the time series, ψ the wavelet function, Δt the time step, and N the series length.

Significance testing employs Gaussian red noise background models with specified autocorrelation. The null hypothesis is a stationary χ^2-distributed process, where peaks exceeding confidence levels indicate significant periodicities.

Applied to J0811.4+0146, the WWZ reveals a significant (~4.15 yr) quasi-periodic oscillation (Figure 3), demonstrating its utility for detecting evolving blazar periodicities.

3.3 Discrete Correlation Function (DCF)

The DCF method identifies periodicities in astronomical time series [**?**]:

$$\mathrm{DCF}(\tau) = \frac{1}{M} \sum_{i,j} \frac{(a_i - \bar{a})(b_j - \bar{b})}{\sigma_a \sigma_b} \tag{2}$$

where τ is time lag and M is pair count. Analysis of J0811.4+0146 reveals a primary period of ~1450 d and its harmonic at ~2900 d (Fig. 4).

3.4 Jurkevich (JV)

The JV method [**?**] detects quasi-periods by phase-folding:

$$\overline{\sigma^2}(P) = \frac{1}{N} \sum_{j=1}^{N} \sigma_j^2(P), \quad \phi_i = \frac{t_i \bmod P}{P} \tag{3}$$

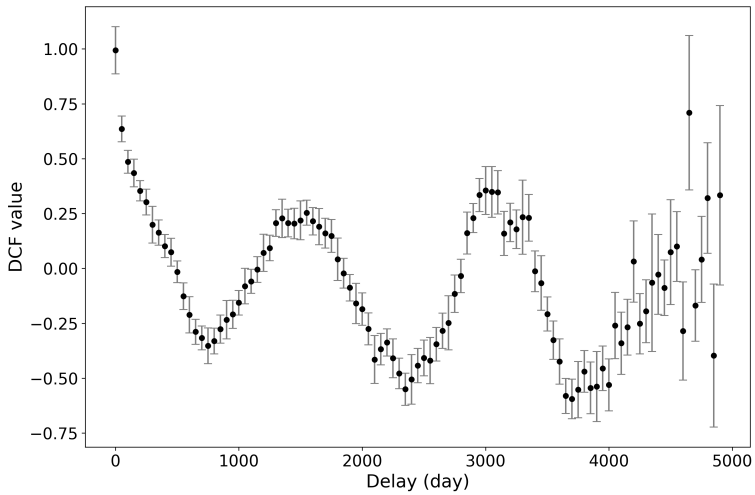

Figure 4: DCF of J0811.4+0146 showing ∼1450 d quasi-period and harmonic.

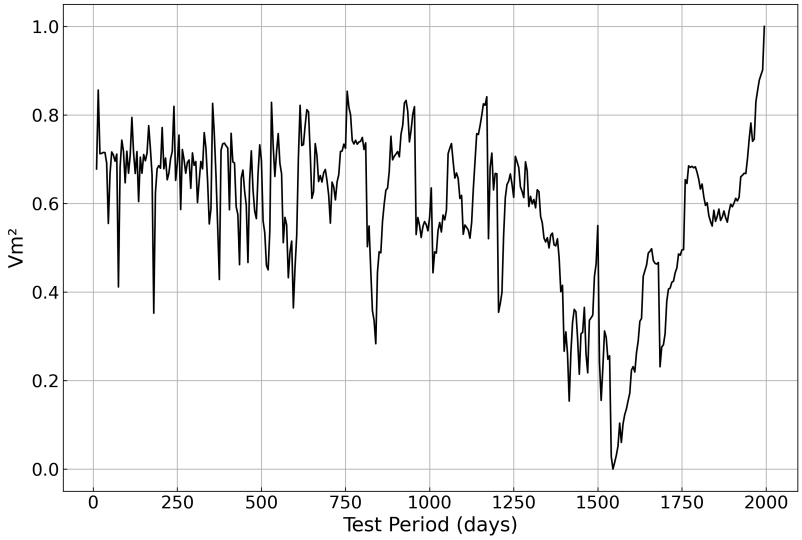

Figure 5: JV analysis of J0811.4+0146 showing ∼1550 d quasi-period.

Minima in $\overline{\sigma^2}$ indicate periods. For J0811.4+0146, the strongest minimum occurs near ∼1550 d (Fig. 5).

3.5 Error estimation

Period uncertainties were determined using 10^4 Monte-Carlo surrogate light curves with Gaussian noise [5, 10]. Errors in Table 1 are standard deviations of period distributions across algorithms. The significance of the primary LSP peak (1594 d) was tested against 10^4 red-noise surrogates (broken power-law PSD: $\beta_1 = 1.3$ for $f < 1/1200\,\mathrm{d}^{-1}$, $\beta_2 = 2.1$ for $f >$). The peak exceeds 99.99966% confidence (4.5σ, FAP=3.4×10^{-6}).

4. Results and Discussion

Analysis of J0811.4+0146's γ-ray flux (2008-2024) reveals a significant quasi-periodic oscillation (4.5σ) using four independent methods: LSP, WWZ, DCF, and JV (Table 1). The LSP-derived period of 4.35 ± 0.34 yr serves as our primary result due to its conservative false-alarm probability [**?**].

The methods show consistent periods within uncertainties: WWZ (4.15 ± 0.42 yr), DCF (3.97 ± 0.30 yr), and JV (4.25 ± 0.11 yr). This agreement confirms a robust quasi-periodicity. Minor variations arise from methodological differences in handling data characteristics like sampling and noise.

Table 1: QPO and its errors of J0811.4+0146 obtained by different time-series analysis methods: Lomb-Scargle Periodogram (LSP), Weighted Wavelet Z-transform (WWZ), Discrete Correlation Function (DCF), and Jurkevich (JV).

Method	Period (Year)	Statistical Error (Year)
LSP	4.35	0.34
WWZ	4.15	0.42
DCF	3.97	0.30
JV	4.25	0.11

In this work we analyse the most complete *Fermi*–LAT data set so far (2008–2024, 15.3 yr) for J0811.4+0146. Using four independent time–series tools (LSP, WWZ, DCF, JV) we detect a consistent quasi-periodic oscillation of $P_\gamma = 4.35 \pm 0.34$ yr, now spanning almost four full cycles (Table 1). Seven- and 30-day binned light curves confirm that the signal is insensitive to the choice of bin size. The gain in significance over earlier claims stems from the longer baseline and the cross-validation of multiple techniques.

Quasi-periodicity is not unique to this source. Among FSRQs, S5 1044+71 (3.1 ± 0.4 yr), PKS 0426−380 (3.7 ± 0.5 yr) and J0351−1153 (3.7 ± 0.5 yr) exhibit similar cycles, plausibly linked to accretion-disk or BLR modulation. BL Lac objects often show even stronger signals: the HBLs PG 1553+113 (2.2 ± 0.1 yr) and PKS 2155−304 (1.7 ± 0.1 yr) are textbook cases, while the LBL J0428.6−3756 (3.35 yr) may reflect a binary–black-hole origin. Observed QPOs thus span days to years, with short periods likely arising from inner-disc processes and long periods favouring jet precession in a super-massive binary system.

Considering both relativistic time dilation and cosmological expansion, the intrinsic QPO period in the jet ($P_{\rm jet}$) is related to the observed period ($P_{\rm obs}$) by

$$P_{\rm jet} = \frac{2\,\Gamma\,P_{\rm obs}}{1+z}, \tag{4}$$

where $\Gamma = 10.5$ is the Lorentz factor for J0811.4+0146 and z is its redshift. Substituting these values yields $P_{\rm jet} \simeq 42.49$ yr.

According to [**?**], the periodicity is caused by the spiral motion driven by the orbits of the black holes for periods greater than 10 days, and by the rotation of the internal jets for periods less

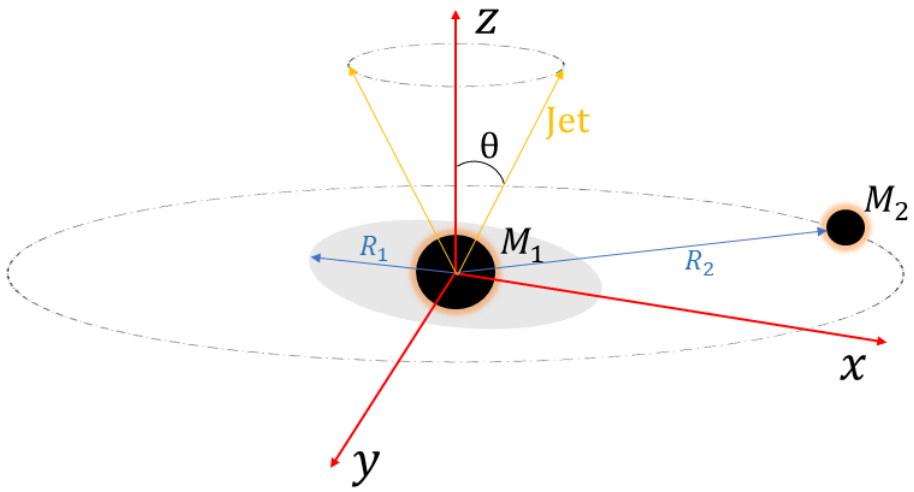

Figure 6: SMBHB model for explaining this QPO of J0811.4+0146. The grey region represents the accretion disk of the primary black hole, which is not coplanar with the orbital plane. The yellow arrows represent the jets, which periodically process in a direction perpendicular to the accretion disk.

than 10 days. If the observation period is longer than one year, the Newtonian-driven jet precession caused by rigid body precession in the accretion disk should be considered. Therefore, this paper considers that the observed period of 4.35 yr is explained by Newtonian-driven jet precession. The model selected for J0811.4+0146 is Supermassive Black Hole Binary model (SMBHB) , which consists of a primary black hole and a secondary black hole orbiting each other (see Figure 6). The main black hole structure has an accretion disk, and relativistic jets are perpendicular to the accretion disk. When the secondary black hole orbits the main black hole, the secondary black hole will exert gravitational torque on the accretion disk of the main black hole, resulting in periodic disturbance of the accretion disk. The disturbance of the accretion disk will transfer periodicity to the internal relativistic jet, resulting in the jet precession. For the physical process of QPO in SMBHB model, the relationship between the jet cavity period and the orbital period is:

$$\frac{P_{M_2}}{P_{\rm jet}} = \frac{3}{4}\frac{M_2}{M_1}\left(\frac{R_1}{R_2}\right)^{\frac{3}{2}}\left(\frac{M_1}{M_1+M_2}\right)^{\frac{1}{2}}\cos\theta, \tag{5}$$

where M_2 is the mass of the secondary object, and M_1 is the mass of the primary object.

In this system, [**?**] studied the system parameters when the Doppler factor δ was 2, 5 and 10, respectively. They found that when the Doppler factor δ is greater than or equal to 10, the mass of the secondary black hole is less than the mass of the primary black hole. Therefore, the average value of the system parameters when the Doppler factor $\delta = 10$ is adopted as the system parameters of this source. The mass of the primary black hole is $73.3 \times 10^8 M_\odot$, the mass of the secondary black hole is $21.3 \times 10^8 M_\odot$, and $\frac{R_1}{R_2}$ is 0.27, so the orbital period of the secondary black hole P_{M_2} is equal to 1.15 yr. The above analysis shows that periodic flux modulation can be generated when the direction of the jet changes periodically with the direction of the observer's line of sight.

5. Summary

We analyse 15 yr of *Fermi*–LAT data for the BL Lac J0811.4+0146. Four timing tools—Lomb–Scargle, WWZ, DCF and Jurkevich—independently reveal a quasi-periodic oscillation at $P_\gamma = 4.35 \pm 0.34$ yr with $4.5\,\sigma$ significance. Tests with 3-, 7- and 30-day light-curve bins confirm the signal's stability. Interpreting the QPO as jet precession in a binary-black-hole system gives an intrinsic precession period of ~ 42 yr after relativistic and cosmological corrections, comparable to the companion's orbital timescale.

References

[1] YANG S-B et al. *Gaussian process modeling fermi-lat γ-ray blazar variability: A sample of blazars with γ-ray quasi-periodicities* ApJ, 2021, **907**(2): 105.

[2] ABDOLLAHI S et al. *Fermi large area telescope fourth source catalog* ApJS, 2020, **247**(1): 33.

[3] URRY C M and PADOVANI P. *Unified schemes for radio-loud active galactic nuclei* PASP, 1995, **107**(715): 803.

[4] ZHANG B-K et al. *The optical spectral features of 27 Fermi blazars* MNRAS, 2023, **519**(4): 5263–5270.

[5] TIMMER J and KOENIG M. *On generating power law noise* A&A, 1995, **300**: 707.

[6] GUIDORZI C. *Power-density spectrum of non-stationary short-lived light curves* MNRAS, 2011, **415**(4): 3561–3570.

[7] VANDERPLAS J T. *Understanding the lomb–scargle periodogram* ApJS, 2018, **236**(1): 16.

[8] FOSTER G. *Wavelets for period analysis of unevenly sampled time series* ApJ, 1996, **112**: 1709–1729.

[9] TORRENCE C and COMPO G P. *A practical guide to wavelet analysis* BAMS, 1998, **79**(1): 61–78.

[10] COVINO S et al. *Looking at blazar light-curve periodicities with gaussian processes* ApJ, 2020, **895**(2): 122.

[11] FEIGELSON E D et al. *Autoregressive times series methods for time domain astronomy* Frontiers in Physics, 2018, **6**: 80.

[12] RICHARDS J L et al. *Connecting radio variability to the characteristics of gamma-ray blazars* MNRAS, 2014, **438**(4): 3058–3069.

[13] PALMER D M. *A fast chi-squared technique for period search of irregularly sampled data* ApJ, 2009, **695**(1): 496.